Microbial synthesis of core/shell gold/palladium nanoparticles for applications in green chemistry.

Deplanche, K; Merroun, ML; Casadesus, M; Tran, DT; Mikheenko, Iryna; Bennett, JA; Zhu, J; Jones, IP; Attard, GA; Wood, Joseph; Selenska-Pobell, S; Macaskie, Lynne

DOI:
10.1098/rsif.2012.0003

Document Version
Peer reviewed version

Citation for published version (Harvard):
Deplanche, K, Merroun, ML, Casadesus, M, Tran, DT, Mikheenko, I, Bennett, JA, Zhu, J, Jones, IP, Attard, GA, Wood, J, Selenska-Pobell, S & Macaskie, L 2012, 'Microbial synthesis of core/shell gold/palladium nanoparticles for applications in green chemistry.', *Journal of The Royal Society Interface*.
https://doi.org/10.1098/rsif.2012.0003

Microbial Synthesis of core/shell Gold/Palladium Nanoparticles for Applications in Green Chemistry

Kevin Deplanche[1], Mohamed L. Merroun[2], Merixtell Casadesus[3], Dung T. Tran[4], Iryna P. Mikheenko[1], James A. Bennett[5], Ju. Zhu[5] Joe.Wood[5] Ian P. Jones[4], Gary A. Attard[3], Sonja Selenska-Pobell[2] and Lynne E. Macaskie[1**]*

[1]Unit of Functional Bionanomaterials, School of Biosciences, University of Birmingham, Edgbaston, Birmingham, B15 2TT, United Kingdom.

[2]Institut für Radiochemie, Forschungszentrum Dresden Rossendorf, P. O. Box 510119, D-01314 Dresden, Germany.

[2*]Present address: Departamento de Microbiologia, Universidad de Granada, Campus Fuentenueva 18071 Granada, Spain

[3]School of Chemistry, Cardiff University, Park Place, Cardiff, CF10 3AT, United Kingdom.

[4]School of Metallurgy and Materials, University of Birmingham, Edgbaston, Birmingham, B15 2TT, United Kingdom.

[5]School of Chemical Engineering University of Birmingham, Edgbaston, Birmingham, B15 2TT, United Kingdom.

Running Head title: microbial synthesis of Au/Pd core/shell nanoparticles

**Correspondence to L.E.Macaskie, Tel (44)-121-414-5889, Fax (44)-121-414-5925, Email L.E.Macaskie@bham.ac.uk

ABSTRACT

A novel biochemical method is reported based on the sacrificial hydrogen strategy to synthesise bimetallic Au/Pd nanoparticles (NPs) with a core/shell configuration. The ability of *E. coli* cells supplied with H_2 as electron donor to rapidly precipitate Pd(II) ions from solution is used to promote the reduction of soluble Au(III). Pre-coating cells with Pd(0) (bioPd) dramatically accelerated Au(III) reduction, with the Au(III) reduction rate being dependent upon the initial Pd loading by mass on the cells. Following Au(III) addition, the bioPd/Au(III) mixture rapidly turned purple indicating the formation of colloidal gold. Mapping of bio-NPs by energy dispersive X-ray microanalysis (EDX) suggested Au-dense core regions and peripheral Pd but only Au was detected by X-ray diffraction analysis. However surface analysis of cleaned NPs by cyclic voltammetry (CV) revealed largely Pd surface sites, suggesting, since XRD shows no crystalline Pd component, that layers of Pd atoms surround Au NPs. Characterisation of the bimetallic particles using X-ray absorption spectroscopy (XANES and EXAFS) confirmed the existence of Au-rich core and Pd-rich shell type bimetallic biogenic NPs. These showed comparable catalytic activity to chemical counterparts with respect to the oxidation of benzyl alcohol, in air, and at a low temperature (90 ^{o}C).

Keywords: bioreduction, bimetallic catalysts, catalysis, core/shell, *Escherichia coli,* gold, palladium

INTRODUCTION

Until recently only chemical and physical synthesis methods were available to produce metallic nanoparticles (NPs) but increasing pressure to develop "clean" nanomaterial synthesis methods has led to a growing interest in biotransformations as a route to controlled growth of nanoscale structures. As a result, the design, synthesis and characterisation of biologically synthesised and stabilized NPs have recently become areas of significant interest. Advantages of using microorganisms as nanofactories are multiple, being environmentally-benign and often cheaper than chemical methods. Biological synthesis of NPs is scalable, offers particle size and shape control and can even be coupled to the remediation of precious metal-containing wastes [1]. Various biological alternative approaches to the manufacture of supported metal clusters have been developed. Biotemplating, a 'bottom-up' approach, uses highly ordered biomolecules such as DNA and proteins (e.g. microtubules, bacterial S-layer proteins, flagellin) to grow metal clusters [2-4]. Bioreductive routes utilise the ability of some bacterial cells to reduce metal precursors enzymatically to the zero-valent state *via* an electron donor [5,6], usually leading to the formation of metallic NPs at the cell surface that exhibit a catalytic behaviour similar or superior to metallic NPs prepared using chemical methods in a wide range of reactions [7-11].

Bimetallic NPs that exhibit a core-shell structure [12] were recently shown to possess increased catalytic activity in several reactions [13-15]. For example, the tuned coverage of Au NPs by small Pt entities was found to maximize Pt efficacy in a fuel cell electrocatalyst[13], while the enhanced utility of Pd/Au bimetallic was shown for selective oxidation reactions[14,15]. Although many physico-chemical techniques have been devised to prepare Pd/Au nanomaterials, the synthesis of non-random Pd/Au alloys with highly ordered controlled atomic distribution remains elusive. The structure of bimetallic combinations, which is dictated by the preparation conditions, is crucial in order to obtain the necessary synergistic interactions which lead to increases in catalytic activity. This work presents a simple, facile,

two-step biochemical and chemical hybrid route to produce ordered Au/Pd core/shell nanostructures with strong catalytic activity in the oxidation of benzyl alcohol.

MATERIALS AND METHODS

Organisms and culture conditions

E. coli MC4100 (provided by Professor J. A. Cole, University of Birmingham, UK) was maintained aerobically at 30 °C on nutrient agar plates (Oxoid Ltd, Basingstoke Hampshire, UK). Precultures (10% inoculum (v/v) from a mid-exponential phase culture grown anaerobically in nutrient broth N° 2 (NB, (Oxoid, UK) containing 50 mM sodium formate) were grown overnight at 37 °C in NB N° 2 under anaerobic respiratory conditions (NB N° 2 supplemented with 0.4% sodium fumarate (w/v) and 0.5% glycerol (v/v), final concentrations) to maximize hydrogenase expression [11].

For Pd(II) and Au(III) bioreduction experiments, cultures of *E. coli* MC4100 were grown as above in 2 L Durham bottles almost filled to the brim with medium (nutrient broth n °2) and sealed with rubber stoppers. Mid-logarithmic phase cultures (OD_{600}=0.5-0.7) were harvested by centrifugation (12 000 g, 15 min), washed three times in 100 ml of degassed MOPS-NaOH buffer (20 mM, pH 7.2), re-suspended in 50 ml of the same buffer and stored at 4 °C as concentrated cell suspensions until use, usually the next day. Cell concentration (mg ml^{-1}) was determined by correlation to a pre-determined OD_{600} to dry weight conversion.

Pd(II) and Au(III) solutions

For the preparation of Pd(0)-coated cells (bioPd), an aqueous Pd(II) solution (2 mM, to pH 2.3 with 0.01 M HNO_3) was made by dissolving an appropriate amount of sodium tetrachloropalladate (Na_2PdCl_4, Sigma-Aldrich, Poole, U.K). Similarly, aqueous Au(III) solutions (1 mM, to pH 2.3 with 0.01 M HNO_3) were made by dissolving hydrogen tetrachloroaurate ($HAuCl_4.nH_2O$), Sigma-Aldrich, Poole, U.K) in pre-acidified distilled water.

Manufacture of biomass-supported Pd/Au nanoparticles

First, *E. coli* cells were palladised for examination as follows. A known volume of concentrated resting cell suspension (see above) was transferred anaerobically into 200 ml serum bottles and an appropriate volume of degassed 2 mM Pd(II) solution was added so that the final ratio (weight of Pd:dry weight of cells) was 1:19 give loading of 5% (w/w) Pd on biomass. Cells/Pd mixtures were left to stand (30 min, 30 °C) before H_2 was sparged through the suspension (200 ml/min; 20 min). During H_2 sparging, the colour of the cell/Pd mixtures went from yellow to grey, indicating the reduction of cell surface-bound Pd(II) into Pd(0). Complete removal of Pd(II) from supernatants was confirmed by the $SnCl_2$ assay (see below). Next, bioPd was recovered by centrifugation (12 000 g, 15 min), washed 3 times in distilled water and resuspended in distilled water so that that the final ratio of Au(III) solution to bioPd suspension was 4:3 (vol/vol). The bioPd suspension was degassed (20 min) and transferred anaerobically into an appropriate volume of H_2-saturated Au(III) solution (by sparging H_2 in the solution 30 min at 200 ml/min) so that the final ratio of Pd:Au was 1:1 by mass). The bioPd/Au(III) mixture was allowed to react overnight in a rotary shaker (150 rpm, 30°C) and supernatants were assayed for residual Pd(II) and Au(III) (see below) to ensure the complete removal of both metal species. The final material was recovered as above, washed 3 times in distilled H_2O, once in acetone and left to dry in air.

Assay of soluble Au(III) and Pd(II)

During bioPd manufacture, complete removal of Pd(II) from solution was confirmed by assaying cell/Pd mixture supernatants for residual Pd(II) spectrophotometrically ($SnCl_2$ method [25]). Removal of Au(III) from test solutions was monitored by the thiamine-phloxine assay [26].

Electron microscopy and Energy Dispersive X-ray Analysis (EDX) of Pd/Au loaded biomass

Following metal deposition, pellets of metal-loaded bacteria were prepared for transmission electron microscopy (TEM). Preparations were rinsed twice with distilled water, fixed in 2.5% (wt/vol) glutaraldehyde, centrifuged, resuspended in 1.5 ml of 0.1 M cacodylate buffer (pH 7) and stained in 1% osmium tetroxide in 0.1 M phosphate buffer, pH 7 (60 min). Cells were dehydrated using an ethanol series (70, 90, 100, 100, 100% dried ethanol, 15 min each) and washed twice in propylene oxide (15 min, 9500 g). Cells were embedded in epoxy resin and the mixture was left to polymerise (24 h; 60°C). Sections (100-150 nm thick) were cut from the resin block, placed onto a copper grid and viewed with a JEOL 1200CX2 TEM; accelerating voltage 80 keV.

For EDX analysis, metallised cells were dispersed in water then deposited on a carbon thin film coating copper TEM grids (Agar Scientific, grid thickness: 20-30 nm). A field emission gun Tecnai F20 microscope operating at 200 kV was used for high resolution (HR) STEM imaging. In the STEM mode the smallest condenser aperture C2 = 3 μm (which lowers the electron dose as well as reducing the beam damage) was used; the C1 lens was set to spot size 8; the electron probe size is smaller than 1 nm; the camera length was 150 mm, chosen to minimize noise and artefacts caused by diffraction contrast and bright- field electrons. An X-Max Silicon Drift Detector (SDD) was attached to the microscope to perform EDX element mapping in STEM mode **(Tran, Ian is this OK?).** This SDD has an active area of 80 mm^2 which is advantageously large to produce high X-ray count-rates, reduce the acquisition time needed, and thus ease the drift problems of nano-scale objects. The specimen was tilted to 18 degrees to maximize the X-ray collection of the detector. Detector controlling, analyzing and processing were performed using the INCA software which also provides the *SiteLock*^{TM} function to automatically correct the drift of the particles.

Surface characterisation of biomass-supported Pd/Au NPs by cyclic voltammetry

The NPs surface initially presented an organic layer that was removed by suspending the powder samples in a 6 M NaOH (p.a. grade) solution for 6 weeks, changing the solution every 2 days and

rinsing with ultrapure water. Subsequently the cleaned NPs were kept in a suspension with ultrapure water. All electrochemical experiments were performed in an electrochemical cell as described previously [27]. All electrolytes were prepared using 18.2 MΩ·cm Milli-Q water and Suprapur (Aristar) grade H_2SO_4. Electrolyte solutions were degassed (30 min) before each experiment using oxygen free nitrogen. A Pd-hydrogen reference electrode was utilised in all experiments; all data are given in reference to this electrode unless otherwise stated. Data acquisition was carried out as described previously [27]. For the electrochemical measurements, 10 μL of a cleaned NPs suspension were deposited on a glassy carbon (GC) support electrode. The NPs were allowed to deposit under gravity on top of the electrode and allowed to dry in air to form a homogeneous layer. After the NPs were dried, the electrode was gently rinsed with ultrapure water. Electrolyte solution for electrochemical characterisation consisted of 0.1 M H_2SO_4. All surface characterisation measurements were performed at 100 mV/s and the potential range was from 0.1 V to 1.5 V (vs. Pd/hydrogen) unless otherwise stated.

X-ray absorption spectroscopic characterisation of Pd/Au NPs

Palladium K–edge and gold L_{III}-edge X-ray absorption spectra were collected at the Rossendorf Beamline (ROBL) located at the European Synchrotron Radiation Facility (ESRF), Grenoble (France) using a Si(111) double-crystal monochromator and Si-coated mirrors for focusing and rejection of higher harmonics. Data were collected at room temperature in transmission or in fluorescence mode using argon (Ar)-flushed ionisation chamber or a 13-element Ge detector, respectively. The energies were calibrated by measuring the Pd K-edge and Au L_{III}-edge transmission spectra of Pd and Au foil and defining the first inflection point as 24350 and 11919 eV respectively. The Pd/Au loaded sample was measured as dry sample (powder). The EXAFS oscillations were isolated from the raw, averaged data by removal of the pre-edge background, approximated by a first-order polynomial, followed by μ_0-removal *via* spline fitting techniques and normalization using a Victoreen function. Dead-time correction was applied to fluorescence data. The amplitude reduction factors were obtained to be 0.88

for Pd and 0.92 for Au by fits of the referenced foils, and fixed in the analysis of the EXAFS spectra. The shift in threshold energy, ΔE_0, was varied as a global parameter in the fits. The theoretical scattering phase and amplitude functions used in data analysis were calculated using the FEFF8 [28]. For the Pd edge EXAFS spectra, data for phase-shifts and backscattering-amplitudes were obtained from the PdO (Pd-O scattering) and Pd foil (Pd-Pd scatterings) reference compounds. The Au-Pd reference file used for fitting the Au edge EXAFS spectrum of the experimental sample was determined by a theoretical calculation.

During the fits of EXAFS spectra and in order to reduce the number of fitted variables the following constraints were applied:

The bond distance and Debye-Waller factors for Pd-Au bonds were constrained to be equivalent for both Pd and Au edge.

The ratio of coordination numbers of Pd-Au and Au-Pd pairs must be related to the overall composition of Au and Pd in the sample: $N_{AB} = x_B/x_A$ x N_{BA}, where A and B are the absorbing atoms and x_A and x_B are the molar concentrations of Pd and Au in the sample) [29].

Testing of catalytic activity of the Pd/Au NPs on dried bacteria

Samples prepared as above (here to 2.5%Pd/2.5%Au (wt/wt) on the bacteria) were tested for catalytic activity in a 50 ml Parr 4592 batch reactor loaded with 50 ml benzyl alcohol and 180 mg catalyst. The reactor was sealed and allowed to reach 90 °C before pressurising with air (6 bar), maintained at a constant value by continually feeding air. Samples were periodically removed using a sample valve, filtered (0.2 μm) and then analysed using a Fisons GC8000/MD800 GC/MS versus commercial standards.

RESULTS AND DISCUSSION

We present a facile, size controlled and cost efficient method to synthesise Pd/Au core/shell nanostructures using *E. coli* which, in contrast to *D. desulfuricans* [30], can grow to high density at scale, and does not produce H_2S, a catalyst poison. NP synthesis relies on the ability of *E. coli* cells to reduce Pd(II) ions enzymatically from a precursor ($PdCl_4^{2-}$ salt) using H_2 as an electron donor [11]. We postulated that pre-palladising cells with a fine layer of Pd(0) would lead to an increase in the rate of Au(III) reduction under H_2 (see Fig. 4, supporting material) and result in the incorporation of Au atoms into the Pd seeds. The combined used of imaging and bulk/surface probing techniques permits detailed molecular and atomic scale structural analysis of the biomass-supported Pd/Au nanostructures. Following the sequential reduction of Pd(II) and Au(III), *E. coli* cells exhibited complete coverage of both the cell surface and the periplasmic space, with some cells showing a small number of intracellular NPs (Fig. 1A). Some large clusters were observed (Fig. 1A); a bimodal size distribution was reported previously for chemically-synthesised Pd/Au NPs [17] and for bioNPs on *D. desulfuricans* [30]. Bimetallic Pd-Au particles of ~16 nm were examined with respect to their Au and Pd distributions as shown by the characteristic X-ray signals from L_α transitions for Au and Pd atoms. In accordance with other work using high-angle annular dark field (HAADF) analysis [30], which produces image contrast dependent on atomic number, Fig 1C shows that Pd agglomerates (arrowed) decorate an Au-rich NP core region, with some Pd detected also between the NPs (encircled). Analysis by X-ray powder diffraction (supporting material, Fig. 5) showed clearly crystalline Au(0), but not Pd(0) components.

Characterisation of the obtained Pd/Au structures using XAS analysis shows an important degree of metal-metal coordination. Combined analysis of cyclic voltammetry (Fig. 2) and EXAFS data obtained at the Pd K- and Au L_{III}-edges (Fig. 3) is consistent with the development of a core/shell structure where surface-exposed Pd atoms decorate a core of Au atoms. Figure 2A shows the voltammetric profile for the bioPdAu preparation. The first cycle shows the presence of Pd oxide and the absence of any Au oxide, i.e. most surface sites are occupied by Pd. Since XRD analysis (Fig. 5, supporting material) showed that Au occupied the bulk sites, the bioPdAu NPs appear to exhibit an Au-Pd core-

shell structure. Pd oxide desorption potentials correspond to those expected from bulk Pd although the full width at half maximum of the peak is somewhat larger than for bulk Pd [16] indicating that there is a significant perturbation brought about by the gold component of the NPs. Further potential cycling engenders changes to the surface associated with both oxidative cleaning of all Pd sites and Pd dissolution [16]. Au oxide stripping peaks are now visible and continue to increase in size as a function of potential cycling. This is completely consistent with continual electrochemical dissolution of Pd covering Au sites (after dissolution of a Pd capping layer). Interestingly, this is the reverse configuration of that predicted according to the sequence of reduction of the precursors, i.e., as Pd(0) seeds were used, surface Au-rich Pd NPs immobilised on cells (Pd core/Au shell NPs) were expected. Simple thermodynamic arguments, based on the lower surface energy of Au and stronger Pd-Pd bonding, would also favour the $Pd_{core}Au_{shell}$ configuration.[18].This is clearly not the case here, as confirmed by CV (Fig. 2). Similar results have been reported in studies where the sacrificial hydrogen strategy was used to generate the Pd/Au NPs [17], where the mechanism was attributed to pre-formed Pd-particles reducing Au(III) (the respective redox potentials are Au^{3+}/Au 1.002V; Pd^{2+}/Pd, 0.83V) to generate Pd^{2+} ions which then relocate around Au nanoparticles and are reduced to Pd(0) via H_2 on the Au-NP surface. The two NPs shown in Fig 1C show different stages of this progression.

XANES analysis of the bioPd/Au sample at both Au and Pd edges shows that while Au is mainly present as Au(0), Pd is present as a mixture of Pd(0) and Pd(II), with a significant dominance of the ionic part (see Fig. 6, supporting information). The decrease of whiteline intensity observed at the Au L_{III}-edge of the experimental sample in comparison to the Au foil sample is indicative of the decrease in the density of unoccupied sites of the Au 5d orbital in the bioPd/Au sample relative to the Au bulk, which is typical of Pd-Au alloy formation [19 20]. To confirm Pd-Au alloy formation and to discern different alloying motifs (random or core-shell-like non random) EXAFS spectroscopy was used. Figure 3 shows the EXAFS spectra of bioPd/Au NPs and reference compounds (Au, Pd foils) at both the Pd K- and Au L_{III}- (Fig. 3A, 3B, left panel) edges along with their corresponding Fourier transforms

(FT) (Fig. 3A, 3B, right panel). Pd K- and Au L_{III} structural parameters including the coordination number of the different paths (Au-Au, Au-Pd, Pd-Pd, Pd-Au, and Au-M; Pd-M (where M is Au or Pd)) of Au, Pd foils and bioPd/Au nanoparticles are summarised in Table 1. The first shell Pd-metal coordination number ($N_{Pd\text{-}M} = N_{Pd\text{-}Au} + N_{Pd\text{-}Pd}$) calculated to be 3.1 ± 0.4 (Table 1) is much smaller (by a factor of 3) than that of Au -metal ($N_{Au\text{-}M} = N_{Au\text{-}Au} + N_{Au\text{-}Pd}$) calculated to be 10.7 ± 0.6. According to Teng *et al.* (2008) [21], the fact that $N_{Pd\text{-}M} < N_{Au\text{-}M}$ indicates that a larger number of Pd atoms segregate to the surface of the nanoparticles and Au atoms are present on the core, since atoms on the surface have fewer neighbours than those in the core. In addition, the environment of Au atoms is highly ordered in the bioPd/Au sample, presumably due to their preferential bonding in the core since no lattice expansion was observed in this sample as the $R_{Au\text{-}Au}$ in Au foil and bioPd/Au were similar within the experimental errors. We conclude the EXAFS fitting results are completely in accordance with a Pd shell and Au core structure since N(Au-M)>> N(Pd-M) (Table 1). Additional evidence for the formation of a non-random alloy with a core/shell structure is the fact that the Au-Pd bond length (2.75 ± 0.02 Å) is smaller than those observed for Pd-Pd (2.76 ± 0.02 Å) and Au-Au (2.84 ± 0.02 Å). As suggested previously [21], Au-Pd bonds possibly formed very stable bridges between two sub-lattices at the interface of the ordered Au core and disordered Pd shell structure. The disorder in the Pd shell is due to the bonding of Pd atoms with O as was demonstrated by EXAFS spectroscopy which indicates that the Pd surface atoms are exposed/coordinated to oxygen and/or nitrogen donor atoms since significant contribution to the EXAFS signals arose from those of Pd-O or Pd-N bonds. EXAFS spectroscopy cannot distinguish between the Pd-O and Pd-N contribution; therefore they are both modeled as Pd-O for simplicity. Thus, at the Pd edge, the first three peaks of the FT correspond to Pd-O_1, Pd-O_2 and Pd-Pd bonds, respectively. The distances were identified using Pd-O and Pd-Pd backscattering phase and amplitude functions obtained from atomic coordinates of PdO using the FEFF 8 program. From the Pd-O coordination numbers, the fraction of oxidized atoms was estimated to be about 65% (1.2/1.9).

The size of the bimetallic nanoparticles, estimated by means of the determination of the average metal coordination number, N_{M-M}, where N_{M-M} is 7.8 ± 0.6, corresponds to a particle size of 1.5 to 2.5 nm using a previously reported correlation between the coordination number and the particle size [22]. This is not consistent with particle size estimation obtained from the XRD spectrum (estimated particle size of about 4.5 nm (see Fig. 5, supporting information)) due probably to the enhanced surface disorder (significant relaxation under influence of ligands, e.g. oxygen donor atoms), which may result, according to Yevick and Frenkel [23], in the underestimation of particle size of metal nanoparticles, in the size range under 5 nm.

Finally the catalytic activity of the bioPd/Au NP material was demonstrated. A mass metal loading of 5% is commonly used for chemical catalysts; the NPs (2.5%Pd/2.5%Au) were used to catalyse the oxidation of benzyl alcohol. The results are shown in Table 2, together with values from the literature for the same reaction over conventionally supported catalysts, with supports such as TiO_2[14]. The conditions of the literature experiments varied slightly, although at a high catalyst loading (0.18 g) the TOF for the biogenic catalyst in air (Table 2; entry 1) displayed a slightly higher TOF at 6 bar air pressure than TiO_2 supported catalyst (0.2 g) (Table 2; entry 3) at 2 bar oxygen pressure. However, much higher TOFs can be achieved with TiO_2-supported catalyst than thus far observed for the bioPdAu catalyst but these high activities appear to be favoured by much lower catalyst loadings (~6 x 10^{-5} mol/L in entries 4-8, c.f. ~130-180 x 10^{-5} mol/L; entries 2 and 3) [14, 31, 32]. Higher TOFs of up to 86,500 h^{-1} at a temperature of 433 K have been reported with TiO_2 supported catalyst. According to the Arrhenius effect, increasing the temperature for the biogenic catalyst would also be expected to exponentially increase the rate to values comparable with the maximum TOFs reported in the literature, which will be explored in future investigations.

CONCLUSION

In conclusion, we present a two-step biochemical and chemical hybrid route to produce ordered Au/Pd core/shell nanostructures. First, cells direct the formation of Pd NPs in the periplasm (*via* enzymatic reduction of Pd(II) precursors [(11)]) which are in turn used to seed the formation of Au NPs from solution. Pd(0) seeds reduce Au(III) and Pd relocates as a shell of Pd(0) via a Pd^{2+} intermediate under H_2. The resulting biomass-supported Au/Pd core/shell NPs, and other bimetallics produced using this easy and scalable approach, could potentially find novel applications in diverse fields such as remediation of environmental pollutants [(9)], green chemistry/catalysis (e.g. selective oxidations) and be incorporated in proton exchange membrane fuel cells (PEMFC) *in lieu* of the traditional Pt/Ru catalysts to enhance performances in a cost efficient manner [(10)]. The catalytic activity of bioAu/Pd NPs in selective oxidations has recently been shown in our laboratory [(24)] and is reported here for benzyl alcohol oxidation in air at low temperature..

ACKNOWLEDGEMENT

We acknowledge, with thanks, the support of BBSRC (Grants No BB/C516195/2 and BB/E003788/1) and EPSRC (Grants No EP/D05768X/1 and EP/E034888/1), and the British Council Grant BC-ARC project 1340. We thank A. Scheinost, A, Rossberg and Ch. Hennig from the ROBL Group, ESRF, Grenoble for their help in the EXAFS measurements. This project was supported by the facilities funded through Birmingham Science City: AM2, an AWM supported project part funded by the European Regional Development Fund (ERDF)

Supporting Information Available: Reduction rates of Au(III) by palladized biomass, XRD characterization of the mono and bimetallic preparations, XANES analysis of the Au/Pd nanoparticles, Table with fitting parameters of EXAFS analysis. This material is available free of charge *via* the Internet.

Table 1. Best fits results obtained by EXAFS analysis of Pd foil, Au foil and BioPd/Au bimetallic sample.

Sample	Pd foil	Au foil	BioPd/Au
$N_{Pd\text{-}Pd}$	12[a]	12[a]	1.9(4)
$N_{Pd\text{-}Au}$			1.2[b]
$N_{Au\text{-}Pd}$			0.8(2)
$N_{Au\text{-}Au}$			9.9(6)
$N_{Pd\text{-}M}$			3.1(4)
$N_{Au\text{-}M}$			10.7(6)
[c]$N_{M\text{-}M}$			7.8(6)
$R_{Pd\text{-}Pd}$ (Å)	2.74(14)		2.76(16)
$R_{Pd\text{-}Au}$ (Å)			2.75(17)
$R_{Au\text{-}Au}$ (Å)		2.84(19)	2.84(18)
$\sigma^2_{Pd\text{-}Pd}$ (Å^2)	0.0058(58)		0.0060(6)
$\sigma^2_{Pd\text{-}Au}$ (Å^2)		0.0077(72)	0.0039(4)
$\sigma^2_{Au\text{-}Au}$ (Å^2)			0.0088(9)

[a]Value fixed for calculation

[b]Coordination numbers were constrained in the fits to be varied in accordance with equation: $N_{Pd\text{-}Au}/N_{Au\text{-}Pd} = X_{Au}/X_{Pd}$

[c]$N_{M\text{-}M} = X_{Au}N_{Au\text{-}M} + X_{Pd}N_{Pd\text{-}M}$ (where X_{Au} and X_{Pd} are molar composition of Au and Pd, respectively).

Table 2. Comparison of the catalytic activity of bio-catalyst for benzyl alcohol oxidation with data from literature.

No.	Catalyst 2.5%Au-2.5%Pd on support as shown	Reaction conditions						[Metal] (10^{-5} mol/litre alcohol)		TOF (h^{-1})[a] at 0.5h	Ref.
		Catalyst (g)	Alcohol (l)	*T* (K)	*P* (10^5 Pa)	Gas	*S* (rpm)	Au	Pd		
1	*E.coli*	0.180	0.05	363	6	Air	1200	44.6	82.5	1,083	This study
2	*E.coli*	0.090	0.025	363	1	O_2	1200	44.6	82.5	887	24
3	TiO_2	0.200	0.04	373	2	O_2	1500	63.5	118	607	14
4	TiO_2	0.007	0.04	373	1	O_2	1500	2.1	3.9	6,190	14

a. Calculation of TOF (h^{-1}) after 0.5 h of reaction. TOF (turnover frequency) is defined as molecules reacting per active site in unit time. Here TOF numbers were calculated on the basis of the total loading of metals. P: pressure; S: stirrer speed. Ju give indication of variability…. either number of independent tests and % difference between them or mean and standard error.

FIGURE CAPTIONS

Fig. 1. Electron microscopy of metallised cells of *E. coli* MC4100. (A) TEM of cells of *E. coli* MC4100 following the sequential reduction of Pd(II) and Au(III) (5%/5% Pd/Au on biomass w/w), untreated cells are shown in inset (B); scale bars are 500 nm. (C): EDX mapping of two Pd-Au particles showing superimposed Au and Pd distributions: yellow: X-ray signal intensity from the characteristic L_α transitions of Au; blue: the characteristic L_α transitions of Pd. The particle on the right side has

segregation between Pd and Au with a clearly observed Pd-rich region. The particle on the left side shows homogeneous mixing between Pd and Au. Regions of Pd are apparent at the surface of the nanoparticles (arrowed) and some areas between the NPs also indicated the presence of Pd (circled). Individual distributions of Au and Pd, together with complementary high-angle annular dark field microscopy, which provides atomic number contrast, were described previously [(30)].

Fig. 2. Surface analysis of bioPd/Au using cyclic voltammetry (CV). (a) Voltammetric profile of bioPdAu in 0.1 M H_2SO_4 for the first cycle (——), the tenth cycle (-----), the last cycle (·····) and the GC support (— · — · —). Scan rate 100 $mV \cdot s^{-1}$. (b) Voltammetric profile of bioPdAu in 0.1 M H_2SO_4 from scan 10 onwards. The arrows show the increase/decrease of oxide peaks. Scan rate 100 $mV \cdot s^{-1}$.

Fig. 3. EXAFS analysis of bioPd/Au and reference compounds. K^3-weighted EXAFS spectra (left panel) and corresponding FT (right panel) of bioPd/Au sample and reference compound at the (A) Pd K-edge and (B) Au L_{III}-edge.

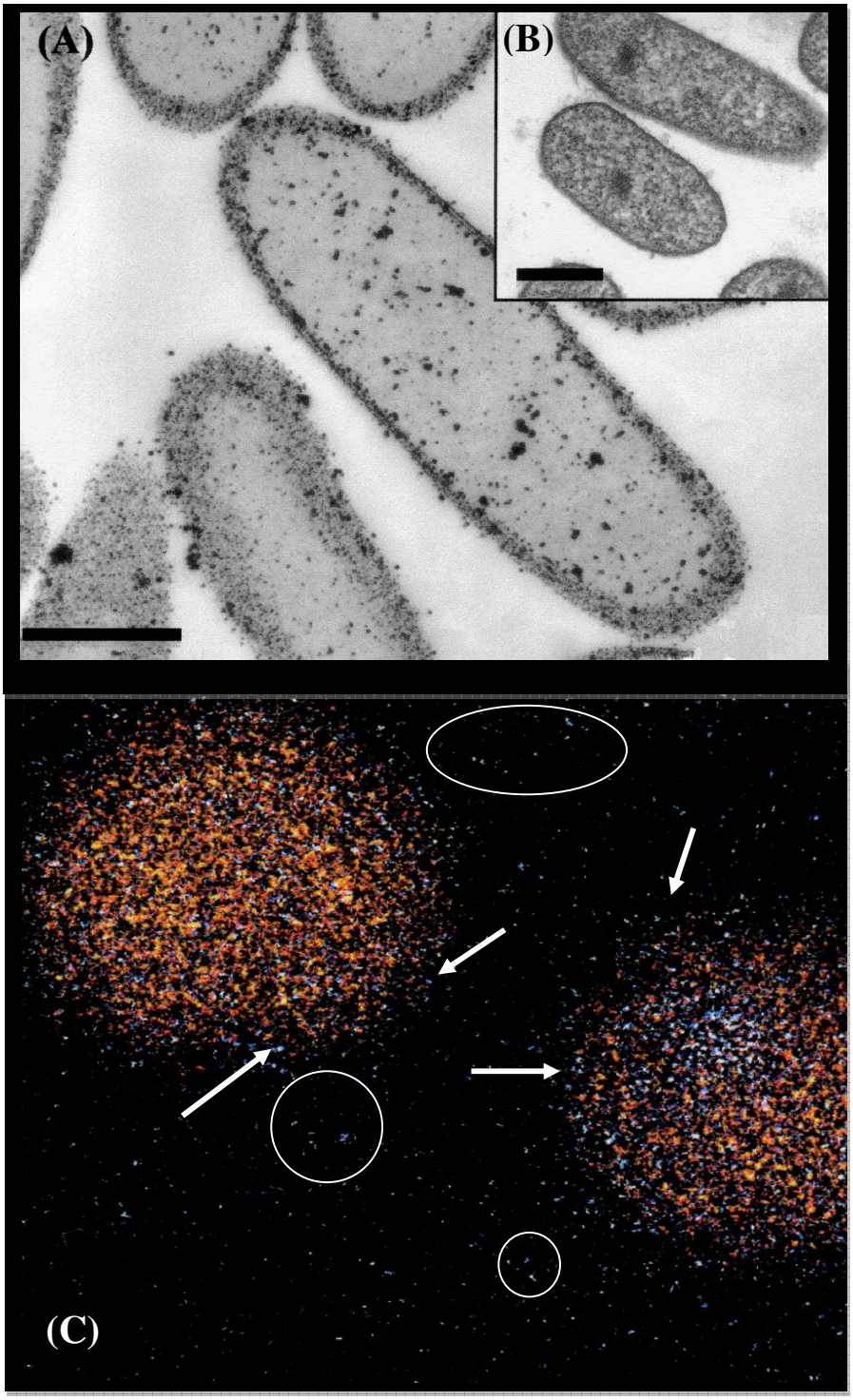

Fig. 1

Fig. 2

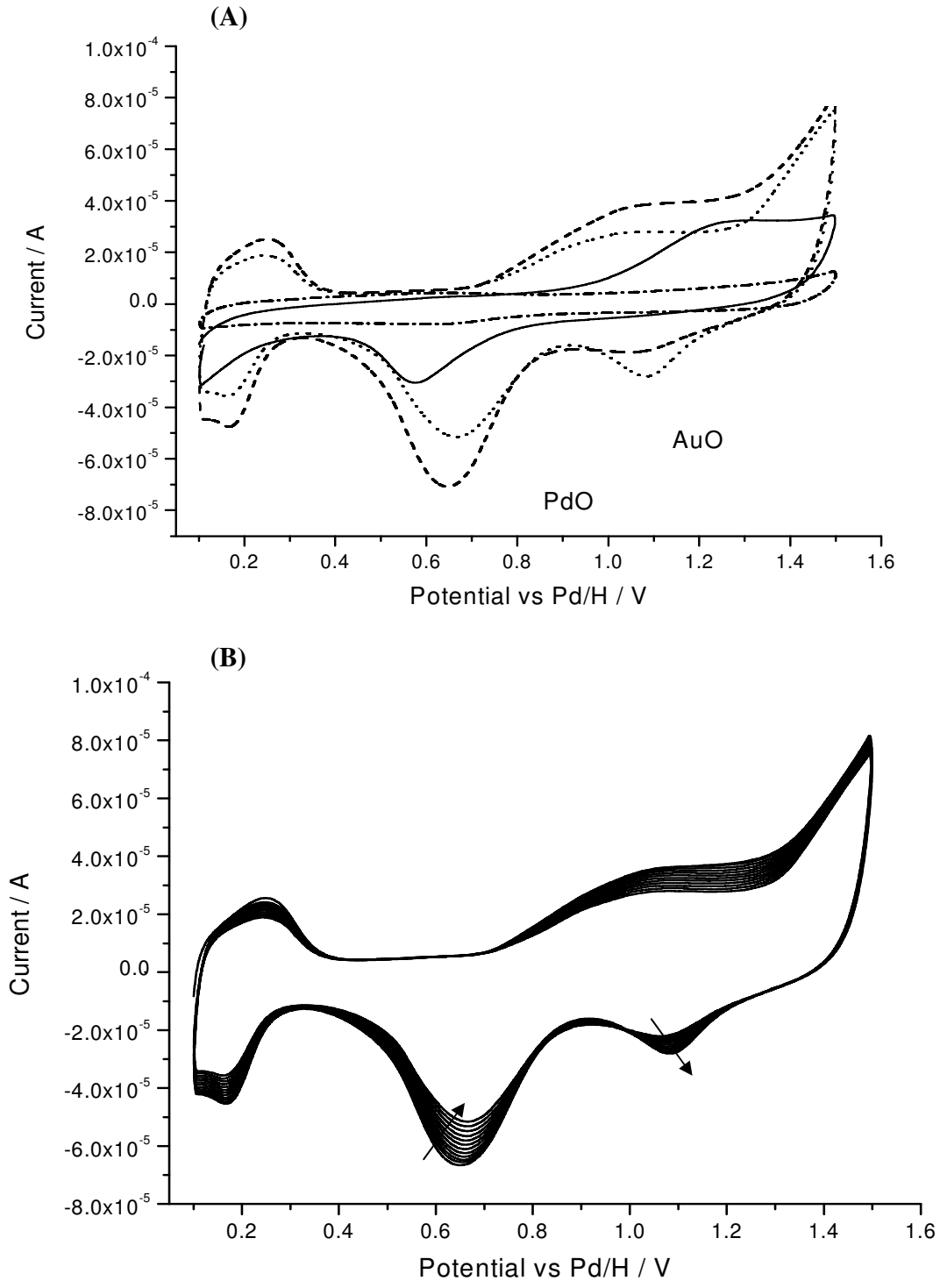
(A)
1.0x10-4
8.0x10-5
6.0x10-5
4.0x10-5
2.0x10-5
0.0
-2.0x10-5
-4.0x10-5
-6.0x10-5
-8.0x10-5
Current / A
AuO
PdO
0.2
0.4
0.6
0.8
1.0
1.2
1.4
1.6
Potential vs Pd/H / V
(B)
1.0x10-4
8.0x10-5
6.0x10-5
4.0x10-5
2.0x10-5
0.0
-2.0x10-5
-4.0x10-5
-6.0x10-5
-8.0x10-5
Current / A
0.2
0.4
0.6
0.8
1.0
1.2
1.4
1.6
Potential vs Pd/H / V

Fig. 3

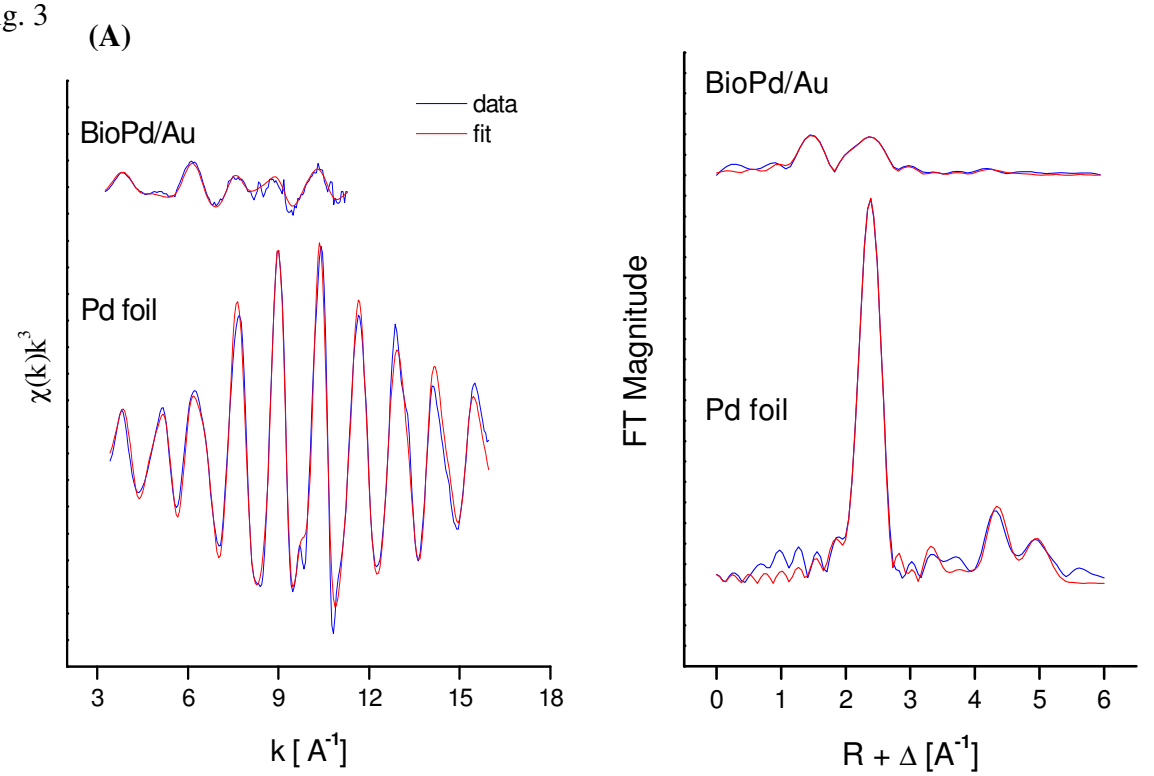
(A)
BioPd/Au
data
fit
Pd foil
χ(k)k³
k [A⁻¹]
FT Magnitude
R + Δ [A⁻¹]

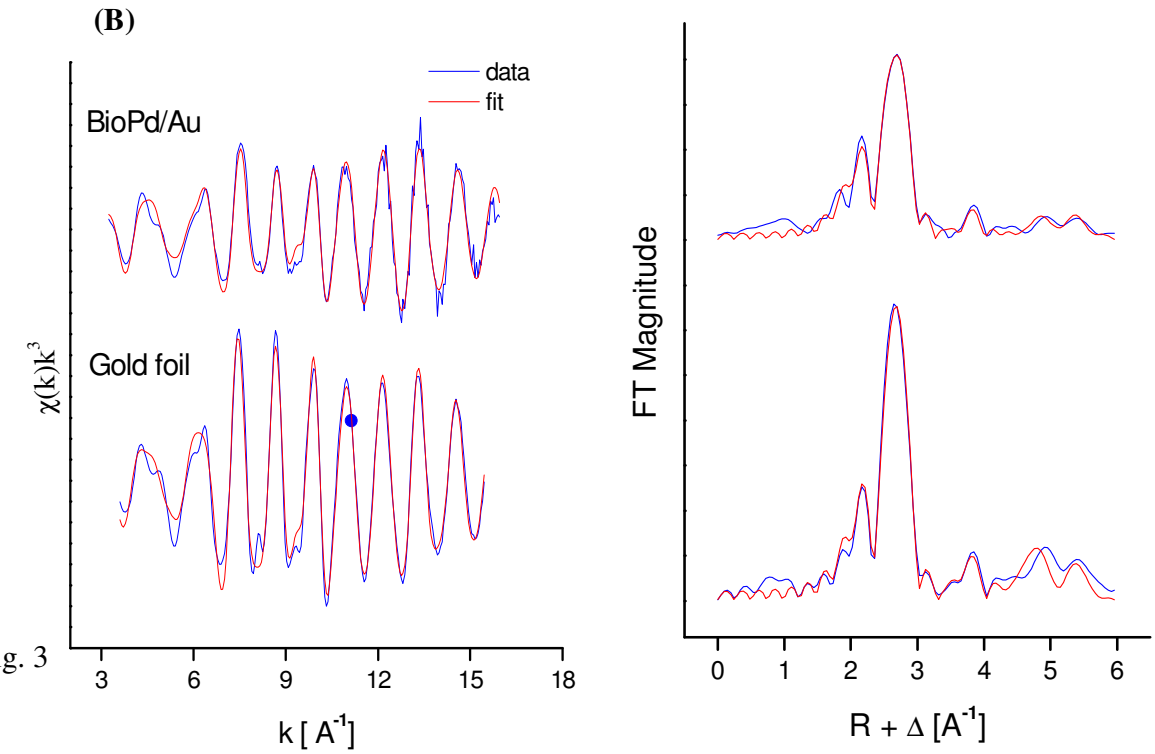
(B)
BioPd/Au
data
fit
Gold foil
χ(k)k³
k [A⁻¹]
FT Magnitude
R + Δ [A⁻¹]

Fig. 3

REFERENCES

1. Mabbett, A. N., Sanyahumbi, D., Yong, P., Macaskie, L. E., Biorecovered precious metals from industrial wastes: Single-step conversion of a mixed metal liquid waste to a inorganic catalysts with environmental application. 2006. *Environ. Sci. Technol*, **40**, 1015–1021.

2. Hall, S. R, Shenton, W., Engelhardt, H., Mann, S., Site-specific organization of gold nanoparticles by biomolecular templating. 2001. *Chem. Phys. Chem.*, **3**, 184-186.

3. McMillan, R. A., Biomolecular templates: nanoparticles align. 2003. *Nature Materials*, **2**, 214-215.

4. Ma, N., Tikhomirov, G., Kelley, S. O., Nucleic acid-passivated semiconductor nanocrystals: biomolecular templating of form and function. 2010. *Acc. Chem. Res.***, 43**, 173-180.

5. Lovely, D. R., Dissimilatory metal reduction. 1993. *Annu. Rev. Microbiol.***, 4**, 263-290.

6. Lloyd, J. R., Yong, P., Macaskie, L. E., Enzymatic recovery of elemental palladium by using sulfate-reducing bacteria. 1998. *Appl. Environ. Microbiol.***, 64**, 4608-4609.

7. Creamer, N. J., Mikheenko, I. P., Yong, P., Deplanche, K., Sanyahumbi, D. *et al.,* Novel supported Pd hydrogenation bionanocatalyst for hybrid homogeneous/ heterogeneous catalysis. 2007. *Catal. Today***, 128**, 80–87.

8. Deplanche, K., Macaskie, L. E., Biorecovery of gold by *Escherichia coli* and *Desulfovibrio desulfuricans*. 2008. *Biotechnol. Bioeng.*, **99**, 1055-064.

9. Deplanche, K., Snape, T. J., Hazrati, S., Harrad, S., Macaskie, L. E., Versatility of a new bioinorganic catalyst: palladized cells of *Desulfovibrio desulfuricans* and application to dehalogenation of flame retardant materials. 2009. *Environ. Technol.*, **30**, 681-92.

10. Yong, P., Mikheenko, I. P., Deplanche, K., Redwood, M. D., Macaskie, L. E., Biorefining of precious metals from wastes: an answer to manufacturing of cheap nanocatalysts for fuel cells and power generation via an integrated biorefinery? 2010. *Biotechnol. Lett.***, 32**, 1821-1828.

11. Deplanche, K., Caldelari, I., Mikheenko, I. P., Sargent, F., Macaskie, L. E., Involvement of hydrogenases in the formation of highly catalytic Pd(0) nanoparticles by bioreduction of Pd(II) using *Escherichia coli* mutant strains. 2010. *Microbiol.***, 156**, 2630-2640.

12. Ferrando, R., Jellinek, J., Johnston, R. L., Nanoalloys: from theory to applications of alloy clusters and nanoparticles. 2008. *Chem. Rev*., **108** (3), 845–910.

13. Zhao, D., Xu, B.-Q., Enhancement of Pt utilization in electrocatalysts by using gold nanoparticles. 2006. *Angew. Chem.***, 118**, 5077–5081.

14 Enache, D. I., Edwards, J. K., Landon, P., Solsona-Espriu, B., Carley, A. F., et al., Solvent-free oxidation of primary alcohols to aldehydes using Au-Pd/ TiO2 Catalysts. 2006. *Science***, 311**, 362-365.

15. Zhou W. J., Lee J. Y., Highly active core-shell Au/Pd catalyst for formic acid electrooxidation. 2007. *Electrochem. Comm.***, 9**, 1725-1729.

16. Rand, D. A. J., Woords, R., Electrosorption characteristics of thin layers of noble metals electrodeposited on different noble metal substrates. 1973. *Electroanal. Chem. Interfac. Electrochem.,* **44,** 83-89 (1973).

17. Kan, C., Cai, W., Li, C., Zhang, L., Hofmeister, H., Ultrasonic synthesis and optical properties of Au/Pd bimetallic nanoparticles in ethylene glycol. 2003. *J. Phys. D: Appl. Phys.***, 36,** 1609–1614.

18. Pittaway, F., Paz-Borbon, L. O., Johnston, R. L., Arslan, H., Ferrando, R., *et al.,* Theoretical studies of palladium-gold nanoclusters: Pd-Au clusters with up to 50 atoms. 2009. *J. Phys. Chem. C***, 113**, 9141-9152.

19. Davis, R. J., Boudart, M., Structure of supported PdAu clusters determined by X-ray absorption spectroscopy. 1994. *J. Phys. Chem.***, 98**, 5471-5477.

20. Reifsnyder, S., Lamb, H., Characterization of silica-supported Pd-Au clusters by X-ray absorption spectroscopy. 1999. *J. Phy.s Chem. B***, 103***,* 321-329.

21. Teng, X., Wang, Q., Liu, P., Han, H., Frenkel, A. I., *et al.*, Formation of Pd/Au nanostructures from Pd nanowires via galvanic replacement reaction. 2008. *J. Am. Chem. Soc***, 130**, 1093-1101.

22. Frenkel, A. I., Hills, C. W., Nuzzo, R. G., A View from the inside: Complexity in the atomic scale ordering of supported metal nanoparticles. 2001. *J. Phys. Chem. B*, ***105*** (51), 12689-12703.

23. Yevick, A., Frenkel, A. I., Effects of surface disorder on EXAFS modeling of metallic clusters. 2010. *Phys. Rev. B*, **81**, 115451-115457.

24. Deplanche K., Mikheenko I. P., Bennett J. A., Merroun M. L., Mounzer H., Wood J., Macaskie L. E. 2011. Selective oxidation of benzyl-alcohol over biomass-supported Au/Pd bioinorganic catalysts. 2011. *Topics in Catal*., **54**: 1110-1114.

25. Charlot G., in *Dosages Absorptiométriques des Éléments Mineraux*, (Masson, Paris, 2nd ed. 1978) 380 p.

26. Deplanche K., L. E. Macaskie, Biorecovery of gold by *Escherichia coli* and *Desulfovibrio desulfuricans*. 2008. *Biotechnol. Bioeng.*, **99**, 1055–1064.

27. Evans R. W., Attard G. A., The redox behaviour of compressed irreversibly adsorbed on Pt(111). 1993. *J. Electroanal. Chem.*, **345**, 337-350.

28. Ankundinov A. L., Ravel, B., Rehr, J. J., Conradson, S. D., Real-space multiple-scattering calculation and interpretation of X-ray-absorption near-edge structure. 1998. *Phys. Rev. B*, **58**, 7565–7576**.**

29. Frenkel, A., Solving the 3D structure of metal nanoparticles. 2007. *Z. Kristallogr*., **222**, 605-611.

30. Tran D.T., Jones I.P., Preece J.A., Johnston R.L., Deplanche K., Macaskie L.E., Configuration of microbially synthesized Pd-Au nanoparticles studied by STEM-based techniques. *Nanotechnol.* 2012 in press.

31. Enache, D.I., Barker, D., Edwards, J.K., Taylor, S.H., Knight, D.W., Carley, A.F., Hutchings, G.J. Solvent-free oxidation of benzyl alcohol using titania-supported gold–palladium catalysts: effect of Au–Pd Ratio on catalytic performance, *Catal. Today* 2007 **122**, 407-411.

32. Miedziak, P.J., He, Q., Edwards, J.K., Taylor, S.H., Knight, D.W., Tarbit, B., Kiely, C.J., Hutchings, G.J. Oxidation of benzyl alcohol using supported gold-palladium nanoparticles, *Catal. Today* 2011 **163**, 47-54.

33. Jaboyedoff, M., Kubler, B., Thelin, P., An empirical Scherrer equation for weakly swelling mixed-layer minerals, especially illite-smectite. 1999. *Clay Minerals***, 34**, 601-617..

SUPPLEMENTARY MATERIAL: SUPPORTING FIGURES

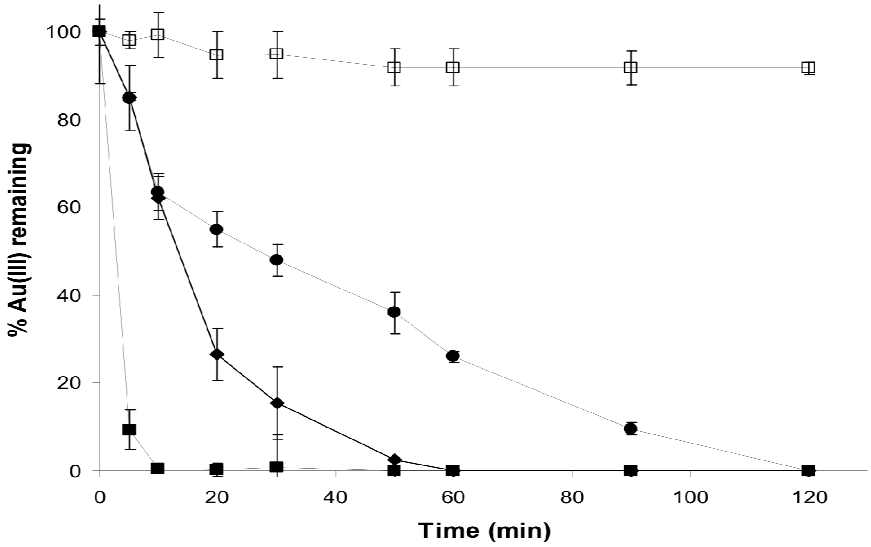

Fig. 4. Reduction of 2 mM Au(III) from $HAuCl_4$ by palladised cells of *E. coli* in the presence of H_2. Following Au(III) addition the bioPd/Au(III) mixture rapidly turned purple indicating the formation of colloidal gold. The increase in Au(III) reduction rate is related to the Pd loading on *E. coli* cells. Reduction of Au(III) by 25% (■) and 5% (♦) bioPd *E. coli* MC4100. The rate of Au(III) reduction using native *E. coli* MC4100 cells (●) and H_2 (□) are shown for comparison. Data are means ± SEM from three experiments. Where no error bars are shown, these were within the dimensions of the symbols. Negligible Au(III) reduction was observed in the absence of cells. Chemical Au(III) reduction using H_2 is typically slow and requires ~4 hours to proceed to completion. The addition of unpalladised (native) resting cells of *E. coli* significantly increased the speed of Au(III) reduction from solution; complete reduction of 2 mM Au(III), pH 2.3 was achieved after ~2 hours of challenge. This value was decreased by half when 5% bioPd was added to the Au(III) solution. Increasing the Pd(0) loading of *E. coli* cells to 25% greatly increased Au(III) reduction rates. More than 90% of soluble Au(III) was lost 5 min upon addition of 25% bioPd and no soluble Au(III) was detected after 10 min of challenge. This represents a twelve fold decrease in the time needed to precipitate 2 mM Au(III) from acidic solution as compared to when using unpalladised *E. coli* cells.

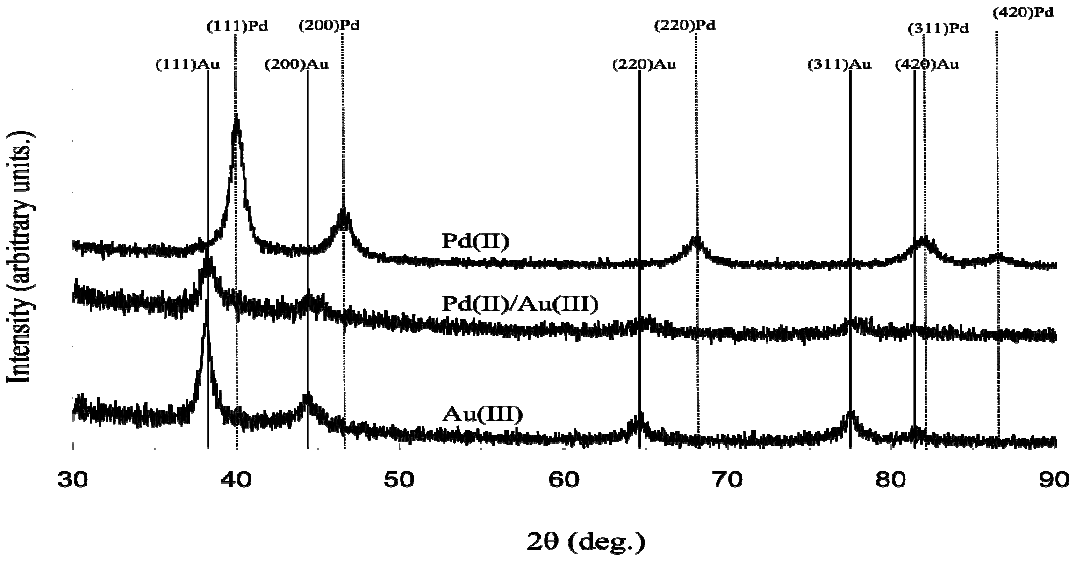

Fig. 5. X-ray powder diffraction (XRD) analysis of monometallic and bimetallic NPs formed by *E. coli* MC4100; X-ray powder pattern of Pd(II)-challenged cells, Au(III)-challenged cells and Pd(II)/Au(III) challenged cells (native or pre-palladised OK Kev?). Ideal positions of bulk Au and Pd are indicated by solid and broken lines, respectively. The cell-mediated reduction of Pd(II) ions and Au(III) ions led to the formation of Pd(0) alone and Au(0) alone, respectively, as no other peaks except those attributable to Pd(0) and Au(0) were detected. The bimetallic pattern replicated the features of the bioAu diffractogram, indicating the absence of large, discrete Pd NPs. The loss of bulk Pd diffraction peaks following Au(III) reduction ((Pd(II)/Au(III) diffractogram) is explained by the fact that most Pd in the bimetallic sample is present as Pd(II) as confirmed by XANES (Fig. 6A). The thickness of the Pd(0) shells surrounding Au(0) cores is probably insufficient to result in detectable Pd peaks in the diffractogram. Similar results for Pd/Au NPs have been reported previously [(29)]. The presence of broad, undefined peaks is a reflection of the poor crystalline state of the material and is typical of NP preparations. The particle size of the cell-bound Pd(0), Au(0) and Pd(0)/Au(0) NPs was estimated using Scherrer's equation [(33)] to be 6.1 ± 0.8 nm, 16.6 ± 1.1 nm and 4.76 ± 1.4 nm respectively.

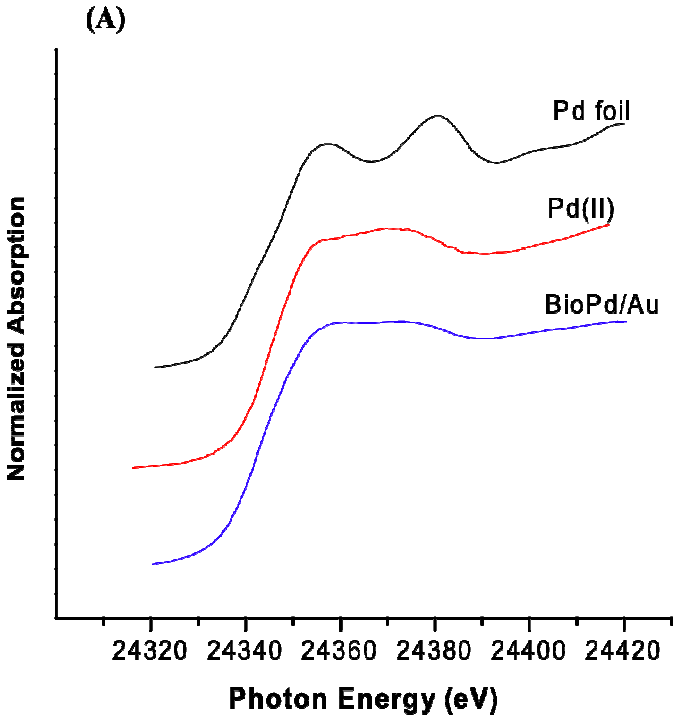
(A)
Pd foil
Pd(II)
BioPd/Au
Normalized Absorption
24320 24340 24360 24380 24400 24420
Photon Energy (eV)

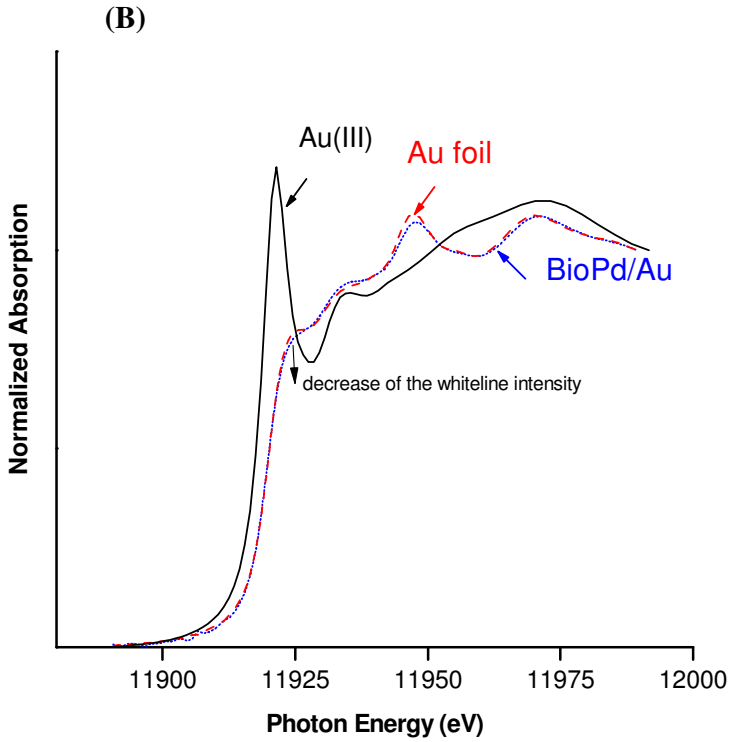
(B)
Au(III)
Au foil
BioPd/Au
decrease of the whiteline intensity
Normalized Absorption
11900 11925 11950 11975 12000
Photon Energy (eV)

Fig. 6. Normalized XANES spectra of bioPd/Au and reference compounds. XANES region of EXAFS spectra at the (**A**) Pd K-edge and (**B**) Au L_{III}-edge. Spectra of reference compounds (Pd(II), Au(III) and Pd and Au foils) are included for comparison. XANES provides information on the average oxidation state and local coordination environment of metals (*20*). Small shifts (a few eV) in XANES absorption edge energies can occur when a metal changes its average oxidation state. Figure 5 shows the XANES regions of the EXAFS spectra obtained for Pd (Fig. 6A) and Au (Fig. 6B) edges. Spectra obtained for the biogenic bimetallic NPs are compared to those obtained for reference compounds under similar conditions. XANES analysis of the bioPd/Au sample at both edges show that while Au is mainly present as Au(0), Pd is present as a mixture of Pd(0) and Pd(II), with a significant dominance of the ionic part.